DOI: 10.1515/amm-2016-0019

A. LISIECKI*,#

EFFECT OF HEAT INPUT DURING DISK LASER BEAD-ON-PLATE WELDING OF THERMOMECHANICALLY ROLLED STEEL ON PENETRATION CHARACTERISTICS AND POROSITY FORMATION IN THE WELD METAL

The paper presents a detailed analysis of the influence of heat input during laser bead-on-plate welding of 5.0 mm thick plates of S700MC steel by modern Disk laser on the mechanism of steel penetration, shape and depth of penetration, and also on tendency to weld porosity formation. Based on the investigations performed in a wide range of laser welding parameters the relationship between laser power and welding speed, thus heat input, required for full penetration was determined. Additionally the relationship between the laser welding parameters and weld quality was determined.

Keywords: Disk laser, welding, thermomechanically rolled steel

1. Introduction

Ongoing efforts to reduce the mass and increase the payload of steel structures, vehicles and machines, lead to wide use of modern high strength steels (HSS) and ultra-high strength steels (UHSS) classified as advanced high strength steels (AHSS) [1÷19].

One grade of such steels is microalloyed steel manufactured during thermomechanically rolling and characterized by fine-grains, and high yield strength up to 700 MPa, e.g. S700MC steel [1÷7].

Manufacturers of the thermomechanically rolled, high yield strength steel S700MC, in addition to outstanding mechanical properties, very high strength, fatigue resistance and toughness, list many other advantages of this steel grade such as excellent weldability and cold forming characteristic, low carbon equivalent CEV 0.38 and CET 0.25, impact strength at least 40 J at -40°C [1÷19, 27].

According to the manufacturers, the low carbon equivalent of S700MC steel and low content of contaminations enable all conventional, both manual and automatic, welding methods to be used. In addition no preheating is required under normal welding conditions and down to joint temperatures of +5°C. Below +5°C preheating to 150°C is recommended. It is also reported that no significant hardness increase appear in the usually narrow heat affected zone, which is of no practical significance [1÷5].

Manufacturers of the microalloyed and thermomechanically rolled steel S700MC provide just a little information about the welding procedures, limiting them only to conventional arc welding methods, mainly to GMAW (gas metal arc welding) or SMAW (submerged metal arc welding) (Fig. 1).

Currently, lasers are increasingly being used as heat sources in welding processes (unconventional welding heat sources). The most modern laser devices of the solid-state lasers, used in welding processes, are disk and fiber lasers [1÷3, 17, 26÷39].

Laser welding, due to high power density of the laser beam and high concentration of the generated heat, allows to weld butt joints having a thickness up to several millimeters without an additional materials, at relatively low heat input and high welding speed. Additionally the thermal cycle of laser welding usually guarantees high cooling rates of the weld metal resulted in very narrow and fine-grained heat affected zone (HAZ). However, in the case of key hole laser welding mode a problem of weld porosity may occur, reported by many researches [1÷3, 17, 36, 33÷39].

The mechanism of laser welding is quite different compared to the arc welding processes. Moreover in a case of laser welding the mechanisms of laser beam interaction with material, intensity of heating, melting and subsequent cooling, penetration depth, width/depth ratio, volume of molten metal may depend on laser beam parameters (laser type), mainly on wave length, power density and also power distribution across the laser beam spot TEM (transverse electromagnetic mode) (Fig. 2) [1÷3, 26, 39- 42].

There is no report so far on the effect of laser welding by Disk lasers on the microstructure and mechanical performance of the fusion zone as well as heat affected zone (HAZ) of the steel grade S700MC. Conditions of laser welding, heat transfer, rates of heating, melting and subsequent rates of cooling and solidification are completely different compared to conventional arc welding methods. Therefore, the detailed study of laser bead-on-plate welding of thermomechanically rolled steel plates S700MC with a thickness of 5.0 mm was carried out by the Disk laser TRUMPF TruDisk 3302.

* THE SILESIAN UNIVERSITY OF TECHNOLOGY, FACULTY OF MECHANICAL ENGINEERING, WELDING DEPARTMENT, 18A KONARSKIEGO STR., 44-100 GLIWICE, POLAND

Corresponding author: aleksander.lisiecki@polsl.pl

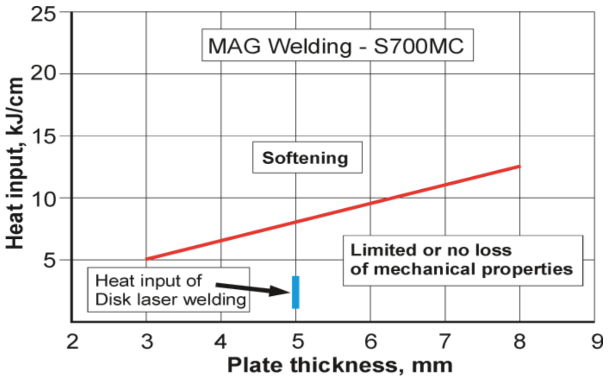

Fig. 1. Recommended heat input during arc welding of steel grade S700MC for different thicknesses of plates

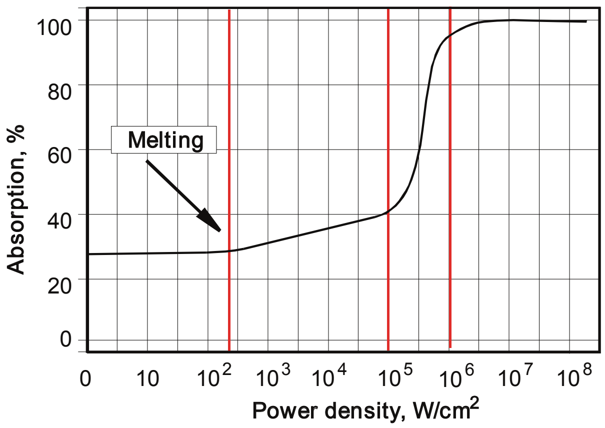

Fig. 2. Relationship between laser radiation absorption and power density of the laser beam

2. Material and experimental procedure

The steel used in the study was thermomechanically rolled, high yield strength steel for cold forming S700MC (according to EN 10149-2, A514 according to ASTM and QStE 690TM according to SEW092) with a thickness of 5.0 mm. The yield strength of the investigated steel should be at least 700 MPa, while the tensile strength can reach up to 950 MPa. The chemical composition of the investigated steel are given in Table 1. Specimens for laser welding tests were cut from 5.0 mm thick plate of S700MC steel into coupons in dimension of 100.0 x 100.0 mm, by means of industrial 2D cutting machine with CO_2 laser. All specimens were sand blasted, and next mechanically cleaned by a brush with stainless steel wires and then chemically cleaned by acetone.

Trials of laser welding were performed using a continuous wave type Disk laser TRUMPF TruDisk 3302 with maximum output power 3300 W (Table 2). The laser beam emitted at 1.03 μm wave length was delivered into the focusing optics via fiber core of 200 μm in diameter and 20 meters long (Fig. 3, Table 2). The laser welding head (focusing optics) was equipped with a 200 mm collimator lens and a 200 mm focusing lens (Table 2).

The beam parameter product (BPP) of the laser beam was < 8.0 mm×mrad. With this configuration of laser optics, the nominal beam spot diameter was 200 μm.

The Disk laser was coupled with a 4-axis fully automated positioning system, which consist of three linear drives in the Cartesian coordinate system "x,y,z" and additionally with a rotary drive axis "a" (Fig. 3).

During the bead-on-plate welding tests the laser beam was focused on the top surface of steel plates (200 μm spot size).

The weld pool was protected by argon flow at 10.0÷12.0 l/min via four cylindrical nozzles 8.0 mm in diameter each (Fig. 3). The shielding nozzles were set in front of the weld pool at an angle 40÷45° to the steel plates surface, ensuring argon flow parallel to the welding direction. Additionally the weld root was protected by argon flow at 3.0 l/min via a grove in a cooper backing placed on the fixture plate (Fig. 3).

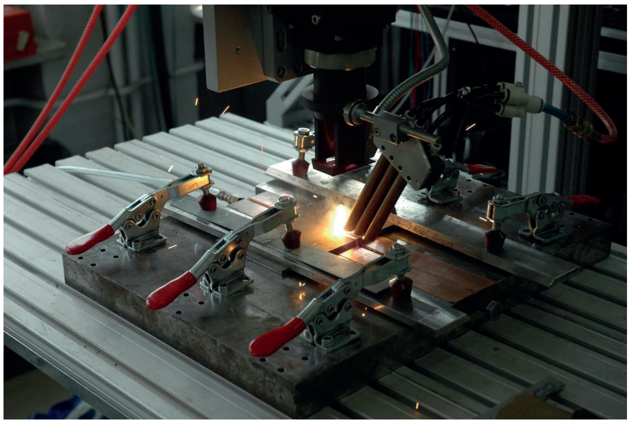

Fig. 3. A view of the bead-on-plate welding of steel S700MC plate by the Disk laser

The bead-on-plate welds were produced as single straight beads at different welding speed and different laser beam power, and thus different heat input, in such a way as to ensure full penetration of the steel plate 5.0 mm thick, with a maximized welding speed and minimized width of face and root of the welds. The test welds were first examined by visual inspection. Next the metallographic examinations were carried out, based on macrostructure and microstructure observations using a light microscope, scanning electron microscope (SEM), and chemical analysis by energy dispersive X-ray spectroscopy (EDS).

Results of the tests, measurements, and analysis are given on the Figs. 3 to 15.

TABLE 1

Chemical composition of thermo-mechanically rolled, high yield strength steel for cold forming S700MC according to EN 10149-3

Content % wt.										
C	Mn	Si	Mo	V	Nb	Ti	Al	P	S	B
max 0.12	max 2.10	max 0.60	max 0.50	max 0.2*	max 0.09*	max 0.22*	max 0.015	max 0.025	max 0.015	max 0.005

*Nb+Ti+V ≤ 0.22 %

TABLE 2
Parameters of bead-on-plate laser welding of the 5.0 mm thick plates of S700MC steel, using the Disk laser TRUMPF TruDisk 3302 (Fig. 3)

Weld bead no.	Output laser power W	Welding speed mm/min (mm/s)	Position of the laser beam focus plane * mm	Heat input J/mm	Width of the weld face mm	Width of the weld root / penetration depth mm	Fusion zone shape	Remarks
1	1000	500 (8.33)	0.0	120	2.5	- / 2.67	V	LF, P, SP, FF
2	1000	200 (3.33)	0.0	300	3.48	- / 2.95	V	LF, NP, FF
3	1500	500 (8.33)	0.0	180	3.4	- / 3.4	V	LF, PS
4	2000	500 (8.33)	0.0	240	3.6	- / 4.22	V	LF, P, ER
5	2500	500 (8.33)	0.0	300	4.0	2.6	X	FP, UF, FF
6	2000	500 (8.33)	+ 3.0	240	3.6	- / 3.65	Y	LF, SP, FF
7	2000	500 (8.33)	- 3.0	240	4.0	- / 4.22	Y	LF, PS, FF
8	**2000**	**300 (5.0)**	0.0	400	4.2	- / 4.7	Y	LF, PS, FF
9	**2000**	**200 (3.33)**	0.0	600	4.4	3.5	X	FP, EW, P, FF
10	2500	750 (12.5)	0.0	200	3.43	1.25	Y	FP, ERR, RP, FF
11	2500	1000 (16.6)	0.0	156	3.3	- / 3.97	Y	LF, P
12	2500	1000 (16.6)	- 1.0	156	2.95	- / 4.09	Y	LF, FF
13	2500	1000 (16.6)	+ 1.0	156	2.61	- / 3.75	Y	LF, P, FF
14	3300	500 (8.33)	0.0	396	5.15	3.9	X	FP, EW, UF, PS, FF
15	3300	1000 (16.6)	0.0	198	3.8	1.7	Y	FP, UF, FF
16	3300	1250 (20.8)	0.0	158,4	2.9	1.4	X	FP, UF, FF, ERR
17	3300	1300 (21.6)	0.0	152.8	4.6	1.97	Y	FP, HF, BF, HR, SI (unstable keyhole)
18	3300	1750 (29.1)	0.0	113.4	2.04	1.1	I	FP, HF, BF, HR, SI (unstable keyhole)
19	3300	2000 (33.3)	0.0	99	1.97	- / 4.1	Y	LF, P, UF, SI

Remarks: * position relative to the top surface of steel plate, other parameters of laser bead-on-plate welding: beam focused on the top surface of joint, wavelength of laser radiation 1.03 µm, focal length of focusing lens: 200.0 µm, focal length of collimator lens: 200.0 µm, fiber core diameter: 200.0 µm, nominal beam spot diameter: 200.0 µm, shielding nozzle diameter: 8.0 µm, shielding gas: Ar (99.999%), gas feed rate on the top surface (face of weld): 10.0÷12.0 l/min, gas feed rate from root side: 3.0 l/min, Quality assessment of the beads: LF – lack of fusion, FP – full penetration, EW – excessive seam width, FF – flat wed face, SI – surface irregularity, UF – undercut of wed face, ER – excessive face reinforcement, ERR – excessive root reinforcement, BF – burn through, HF – hollow face, HR – humped root (due to unstable keyhole), P – porosity, PS – strong porosity, SP – single pore, NP – nest of pores, RP – root porosity

3. Analyze of penetration characteristics and porosity of bead-on-plate welds

The primary aim of the bead-on-plate welding tests and study was to determine the minimum heat input of laser welding, which will guarantee full penetration of the 5.0 mm thick plates of S700MC steel. Trials of bed-on-plate welding, with the laser beam focused on the top surface of steel plate, began with the laser power of 1000 W and welding speed of 500 mm/min, resulted in heat input of 120 J/mm. At this set of laser welding parameters the penetration depth reached just about 50 % of the plate thickness (about 2.5÷2.7 mm) (Fig. 4, Table 2).

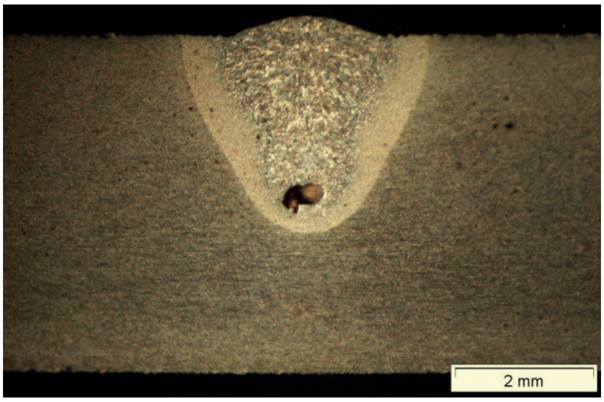

Fig. 4. Macrostructure on cross section of the bead-on-plate weld produced at laser power 1000 W and welding speed 500 mm/min (heat input of 120 J/mm)

Decreasing the welding speed to 200 mm/min resulted in increasing the heat input up to 300 J/mm, but still not enough for full penetration of the steel plate (Table 2). Therefore, the output power of the Disk laser was subsequently and gradually increased at constant welding speed of 500 mm/min (Table 2). Micrographs of the cross sections of investigated bead-on-plate welds are presented on Figures 4 to 8. Although it is clear that bead-on-plate welds, as well as butt joints, consists of a fusion zone (FZ), two symmetrical heat affected zones (HAZ) and base metal (BM) areas, however it is worth mentioning that in the case of investigated welds fusion zones are easy to identify, and also the fusion lines are distinct (Fig. 4, 5). The heat affected zones, their width and the boundary between HAZ and the base metal (BM) are also clear and easy to identify, because of distinctly brighter color of the regions, compared to the BM (Fig. 4, 5).

In the range of output laser power from 1000 W up to 2000 W (heat input from 120 up to 240 J/mm), at constant welding speed of 500 mm/min, faces of partially penetrated bed-on-plate welds are convex, smooth with no undercuts (Fig. 4, 5). However, fusion zones (FZ) of these welds are characterized by "V" shape with porosity mainly in the lower part of weld metal, near bottom of FZ (root porosity), but also in the upper part of FZ (uniform porosity) (Fig. 4, 5). Both, a single pores, as well as clustered porosity were identified in the bottom of these welds (Fig. 4, 5). All the partially penetrated bead-on-plate welds were produced at power density of the laser beam in a range from $3.2x10^6$ W/cm^2 to $6.5x10^6$ W/cm^2, so over the threshold required for keyhole welding of structural mild or low alloyed steel plates [1, 3]. Shape of the analyzed bead-on-plate welds in "V" configuration, as well as the depth/width ratio of FZ in a range 1.15÷1.2 clearly shows that the welds were produced at keyhole mode welding (Fig. 4, 5). In the case of laser keyhole welding of mild steel, as well as stainless steel, and also non-ferrous metals (alloys) such as aluminum, titanium and magnesium, the porosity of weld metal occurs often [40]. A lot of studies on the phenomenon of weld porosity during keyhole laser welding were done. Some of the researchers reported that the intensity and type of weld porosity (uniform, transitional or root) is related mainly to the welding speed. The others found that the porosity is dependent on the weld shape (depth/width ratio), therefore on power density of the laser beam (spot size and focal length) and heat input of laser welding (both welding speed and laser power) [1,3,40, 41]. The main reason of weld porosity, in a case of keyhole laser welding, is instability of the keyhole under certain conditions related to the parameters of welding.

In such conditions the unstable keyhole may easily collapse. Therefore the collapsing liquid metal from the top of keyhole is thought to trap the gases and metal vapors in the solidifying weld metal creating pores in the weld metal (fusion zone) [40, 41].

Further trials of the bead-on-plate laser welding of the 5.0 mm thick S700MC steel plate were continued by increasing the laser power. Increase of the output laser power up to 2500 W (heat input 300 J/mm), at constant bead-on-plate welding speed of 500 mm/min, resulted in full penetration of the 5.0 mm steel plate. Moreover the weld shape was changed into an hour-glass shape ("X" configuration), and no porosity was found on the weld cross-sections, however slight undercuts and concavity of the root were observed (Fig. 5c, Table 2). The reason of this phenomenon (lack of porosity) may be explained by different conditions during solidification of the molten metal inside the keyhole, when the full penetration occurs. Penetration of the laser beam through the whole thickness of the joint allows the laser beam to escape out of the molten pool from the weld root, as well as allows to escape out of the plasma vapors, and gases from the weld root, therefore the susceptibility to form the porosity is limited [40].

In the next step of bead-on-plate welding test the laser output power was kept at the 2500 W, but the welding speed was increased by 50% up to 750 mm/min, resulted in decrease of heat input to 200 J/mm (Table 2). Surprisingly also in this case full penetration was achieved at heat input just 200 J/mm, unlike the welding at lower speed of 500 mm/min, and lower laser power 2000 W, but at significantly higher heat input 240 J/min (Fig. 5b, 6). Furthermore, the fusion zone shape of the bead-on-plate weld produced at 2500 W and 750 mm/min was changed into "Y" shape, compared to the hour-glass shape of the weld produced at lower welding speed. No porosity was found also in this case (Fig. 6). Further increase in welding speed up to 1000 mm/min, at constant laser power of 2500 W, resulted in lack of penetration, but the "Y" configuration of the bead-on-plate weld was maintained (Fig. 7, Table 2).

a) b) c)

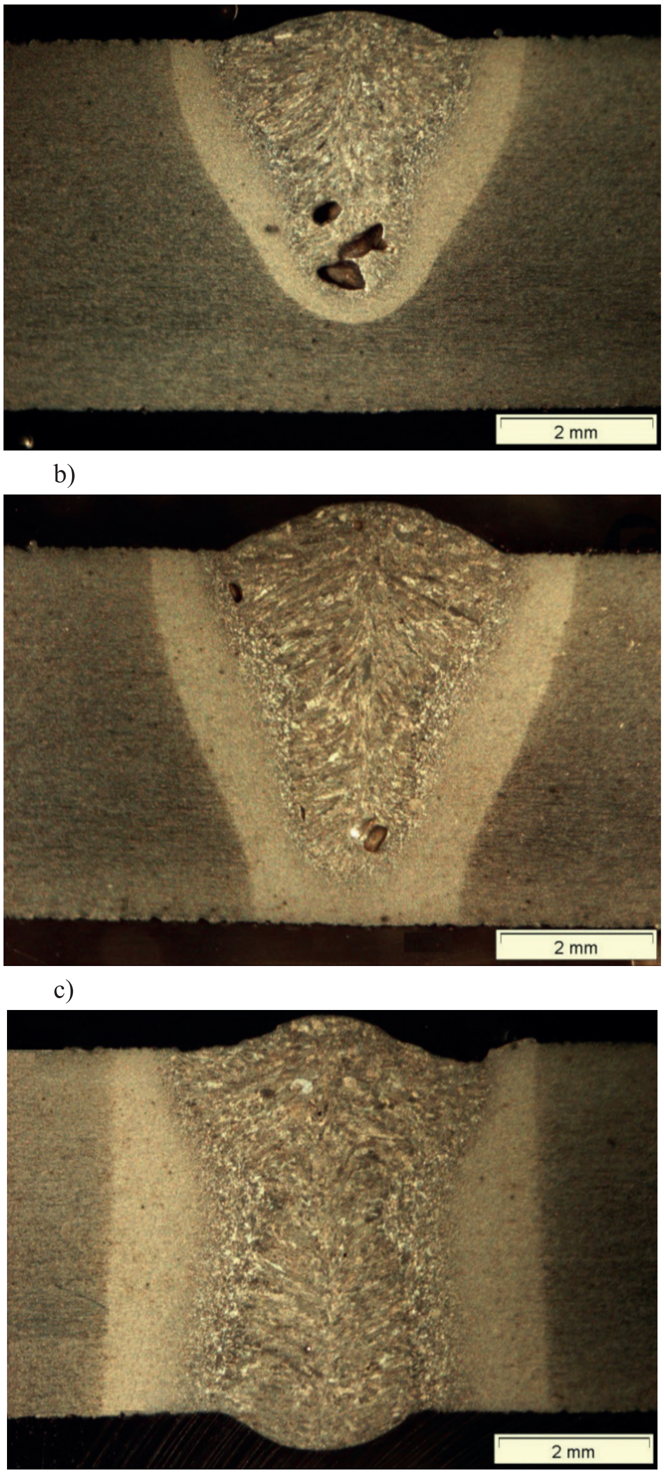

Fig. 5. Macrostructure on cross section of the bead-on-plate weld produced at constant welding speed of 500 mm/min and laser power: a) 1500 W (heat input 180 J/mm), b) 2000 W (heat input 240 J/mm), c) 2500 W (heat input 300 J/mm)

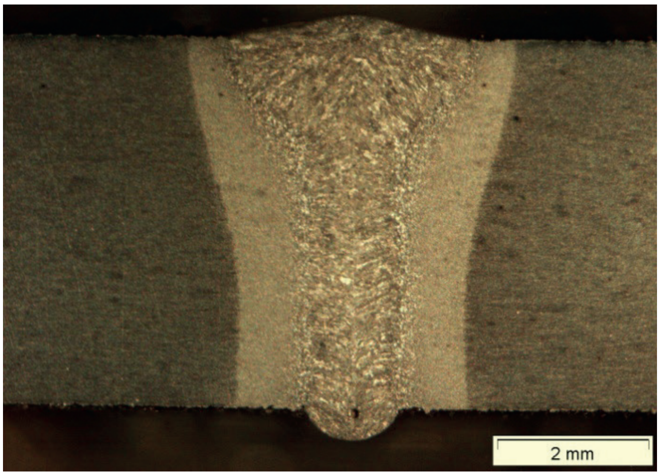

Fig. 6. Macrostructure on cross section of the bead-on-plate weld produced at laser power 2500 W and welding speed 750 mm/min (heat input 200 J/mm)

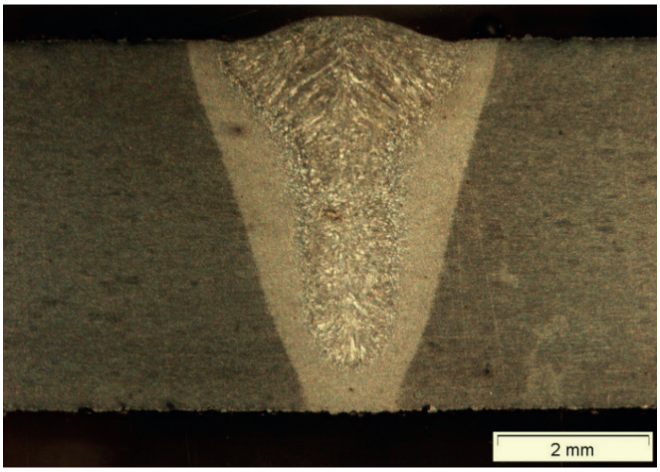

Fig. 7. Macrostructure on cross section of the bead-on-plate weld produced at laser power 2500 W and welding speed 1000 mm/min (heat input 156 J/mm)

Next, in order to determine the maximum welding speed for fully penetrated butt joints of the 5.0 mm thick S700MC steel plates, the subsequent trials of welding were conducted at the maximum laser power 3300 W. The bead-on-plate weld produced at 3300 W and welding speed of 500 mm/min, resulted in heat input nearly 400 J/mm, was characterized by "X" shape configuration, and also by excessive porosity mainly in the root area (Fig. 8, Table 2). The single pores were very large, with a diameter of almost 1.5 mm (Fig. 8).

a)

b)

c)

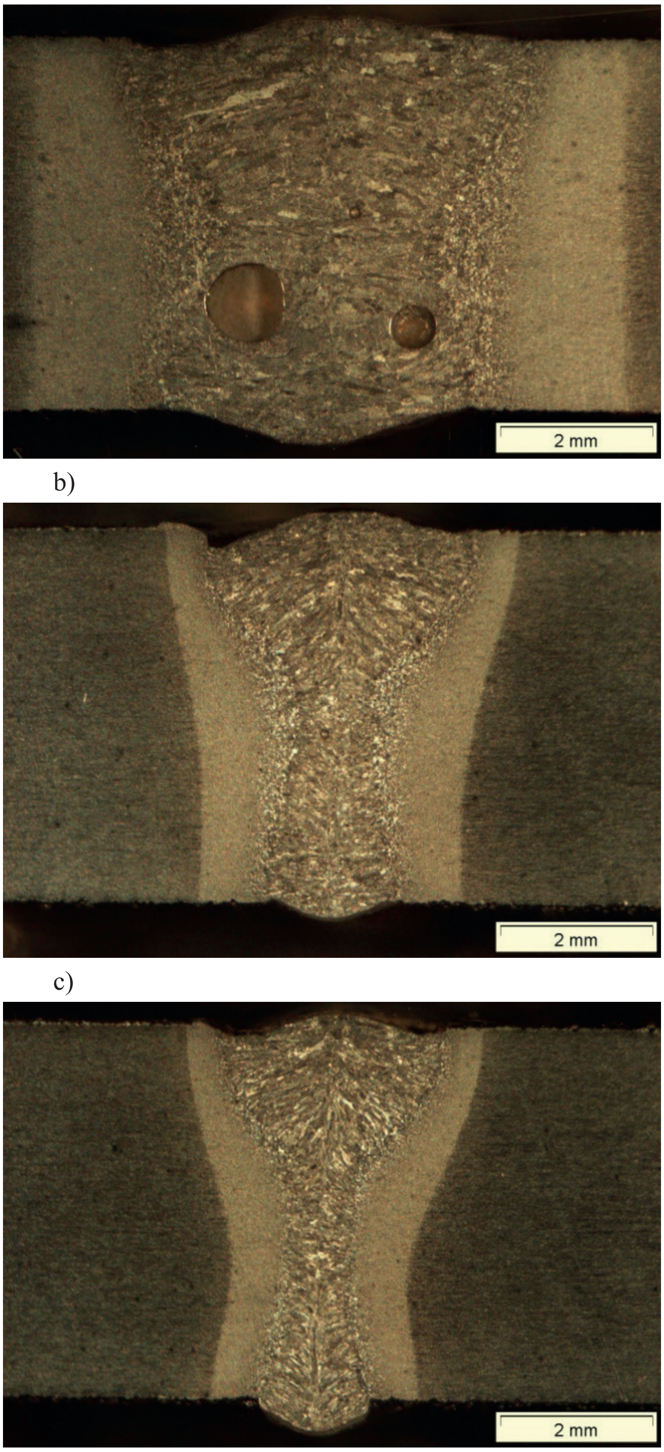

Fig. 8. Macrostructure on cross section of the bead-on-plate weld produced at constant laser power 3300 W and welding speed: a) 500 mm/min (heat input 396 J/mm), b) 1000 mm/min (heat input 198 J/mm), c) 1250 mm/min (heat input 158,4 J/mm)

Doubling of the welding speed, from 500 mm/min up to 1000 mm/min, at maximum laser power of 3300 W (heat input 200 J/mm), resulted in elimination of the porosity evidence in the weld metal (Fig. 8b). FZ of the bead-on-plate weld produced at 3300 W, and heat input of 200 J/mm, was in an hour-glass configuration ("X" configuration) (Fig. 8b). Both face width and the root width were wider compared to the weld produced at the same heat input of 200 J/mm, but at lower power of 2500 W (Fig. 6, 8, Table 2). Further increase of the welding speed up to 1250 mm/min, at maximum laser power of 3300 W, and heat input little below 160 J/mm, resulted in full penetration of the entire length of the weld (Fig. 8c, Table 2). The fully penetrated bead-on-plate weld has an hour-glass shape, and the face width is equal to 3.0 mm, while the width of root is about 1.5 mm (Fig. 8c). Also in this case there was no evidence of weld porosity, however slight undercuts and convexity of the weld face, as well as of the weld root were observed (Fig. 8c).

In the case of heyhole welding by the Disk laser beam, in the investigated range of process parameters, the dependence between a minimum heat input of welding required for full penetration of the 5.0 mm steel plate is a nonlinear relationship, in contrast to the results presented by Rajashekhar S. et al. (Fig. 9) [1]. It was found that the higher output power of the Disk laser beam the lower heat input required for full penetration (Fig. 9).

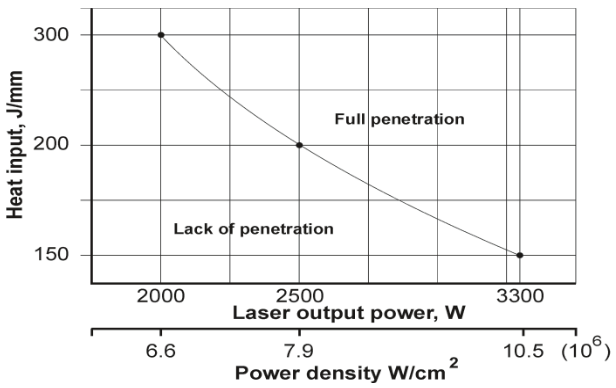

Fig. 9. Relationship between minimum heat input at different laser output power require for full penetration of the 5.0 mm thick plate of steel grade S700MC

Surprisingly it was found that the minimum heat input required for full penetration of the 5.0 mm thick plate of steel grade S700MC, at maximum laser power 3300 W, is just 113 J/mm (Table 2). However, bead-on-plate welding at the maximum laser power and welding speed over 1250 mm/min resulted in extreme instability of the key hole, which in turn resulted in periodic collapsing of the root metal (Fig. 10).

a)

b)

Fig. 10. A view of the humped root of bead-on-plate welds, as a result of key hole instability, produced at 3300 W and welding speed: a) 1300 mm/min (152.8 J/mm), b) 1750 mm/min (113 J/mm)

Trials of bed-on-plate welding with the laser beam defocused (relative to the top surface) showed that defocusing of the laser beam leads to reduction of penetration depth, especially when the laser beam focus is set above the top surface of steel plate (Table 2).

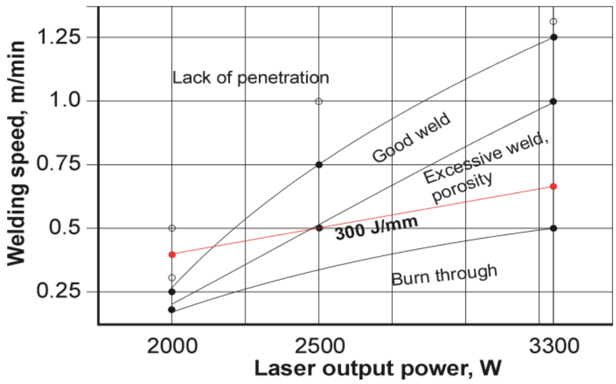

Fig. 11. Influence of the Disk laser output power and bead-on-plate welding speed on weld quality (Table 2)

Based on the wide range of investigations and results, the relationship between laser output power and welding speed for producing good quality weld was determined, and demonstrated on Figure 11.

4. Weld metal and HAZ structure

The microstructure of base metal of microalloyed, thermomechanically rolled steel grade S700MC is shown in Figure 12, while the structures of bead-on-plate welds are shown in Figs. 13 and 14.

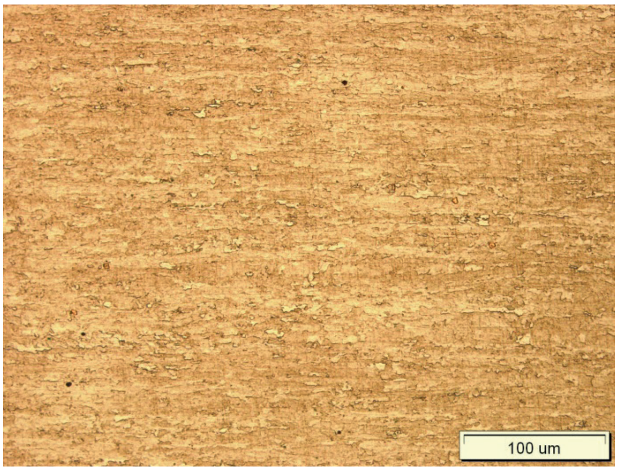

Fig. 12. Microstructure of the base metal of 5.0 thick S700MC steel plate, 3% Nital etched

Base metal is characterized by very fine grains, however there are clear segregation shearing lines, expanding along the plate rolling direction, as a result of inhomogeneous plastic deformation, in subsequent rolling passes. The base metal consists mainly of fine grained ferrite with a uniform dispersion of fine carbides (Fig. 12).

The microstructure of the weld metal (in the FZ), as well as HAZ, was significantly dependent on the heat input of laser welding, and thus subsequent cooling rate. It can be also noticed that the higher the welding speed, even compared to the same level of heat input, the finer the structure of FZ, as well as HAZ (Fig. 13, 14).

The HAZ of bead-on-plate welds, is recrystallized (with no segregation shearing lines) with the structure and grain size dependent on the thermal cycle of laser welding. HAZ structure in the region adjacent to the BM is very fine grained (Fig. 13b, 14b). The very fine grained region reaches about the half-width of the entire HAZ (Fig. 13b, 14b). Structure of the fine grained region of HAZ, similarly as the base metal, is composed of ferrite with a uniform dispersion of fine carbides, but the grain size in this region is about 0.4÷.0.6 µm, significantly smaller that grain size of base metal 0.8÷3.5 µm. On the other hand, the HAZ region adjacent to the FZ boundary (fusion line on the cross-section) is characterized by coarse-grain structure, with dominant acicular ferrite (Fig. 13b, 14b). Moreover, a transitional region may be observed in the HAZ (Fig. 13b, 14b).

a)

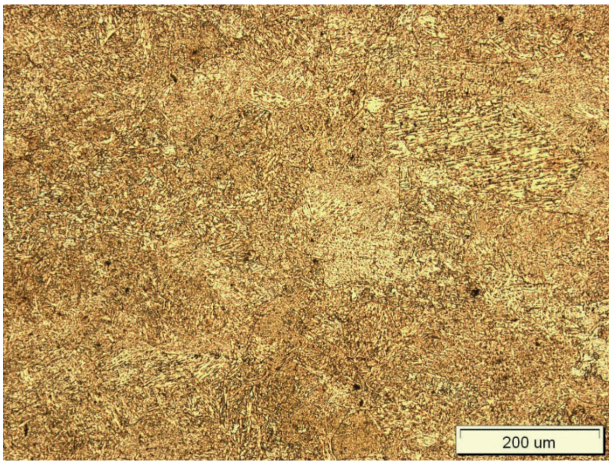

b)

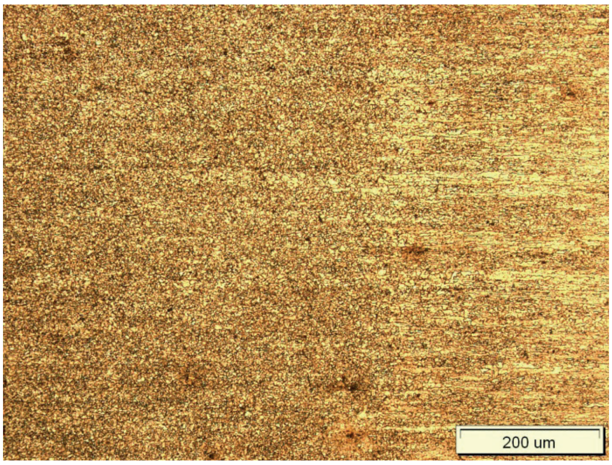

Fig. 13. Microstructure of the bead-on-plate weld produced at laser power 3300 W, welding speed 500 mm/min (396 J/mm); a) fusion zone, b) heat affected zone

Micrographs of the fusion zones of bead-on-plate welds clearly show that the predominant mechanism of weld metal solidification was a heterogeneous, epitaxial nucleation and subsequent epitaxial grain growth (Fig. 13a, 14a). The partially melted grains on the liquid-solid interface (weld pool boundary) were the substrate for nucleation of the columnar grains. Moreover the micrographs of weld FZ show that the columnar grains grow perpendicularly to the liquid-solid interface (fusion line on cross-sections) along the maximum heat conduction (extraction). Orientations of the columnar grains in FZ is dependent on the FZ configurations (shape), thus the parameters of laser welding, mainly heat input (Fig. 13b, 14b). Both in the case of butt joint, and bead-on-plate welds, the columnar grains create a symmetric solidification line at the center (centerline in the mid area of FZ).

a)

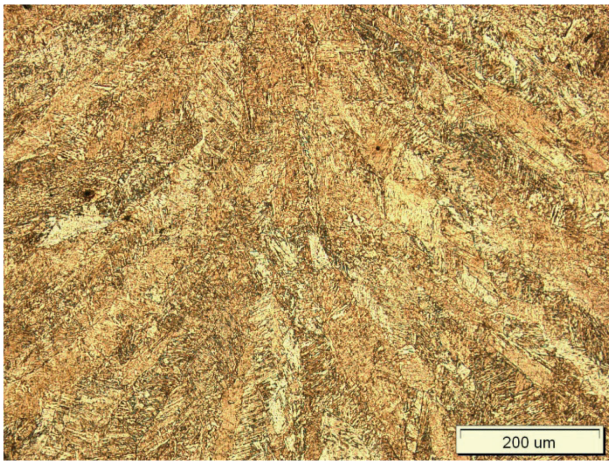

b)

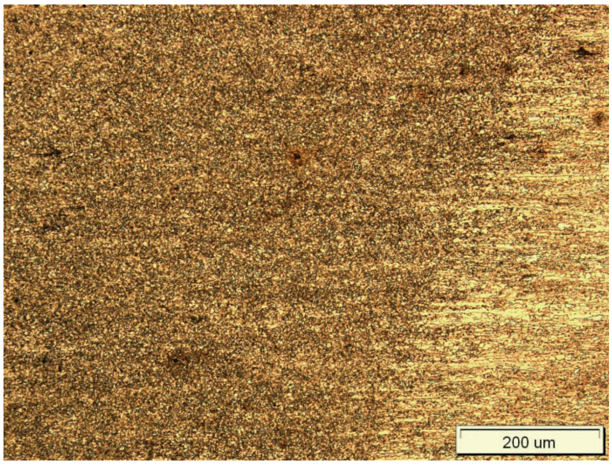

Fig. 14. Microstructure of the bead-on-plate weld produced at laser power 3300 W, welding speed 500 mm/min (396 J/mm); a) fusion zone, b) heat affected zone

Microstructure of weld metal in fusion zone of the bead-on-plate welds consists mainly of acicular ferrite, side plate ferrite, and grain boundary ferrite in proportions dependent on the heat input of laser welding (Fig. 13a, 14a). In a case of the weld produced at the lowest heat input, below 160 J/mm the dominant phase is acicular ferrite, while in the case of the weld produced at excessive heat input 400 J/mm, the dominant phase is side-plate ferrite with a small quantity of acicular ferrite and grain boundary ferrite (Fig. 13a, 14a).

Scanning electron micrograph SEM observations and analysis of the single pores, as well as the clustered porosity, reveled presence of small inclusions and micro cracks on the bottom of pores (Fig. 15a). The EDS spectra of small inclusions show high content of oxygen in the compounds, indicating oxide nature of the inclusions, probably mainly FeO (Fig. 15b). All the inclusions were placed in small areas on a bottom of single pores (Fig. 15a). Increased oxide content in weld metal is probably caused by interference of gas shielding by plasma plume during instability of the key hole.

a)

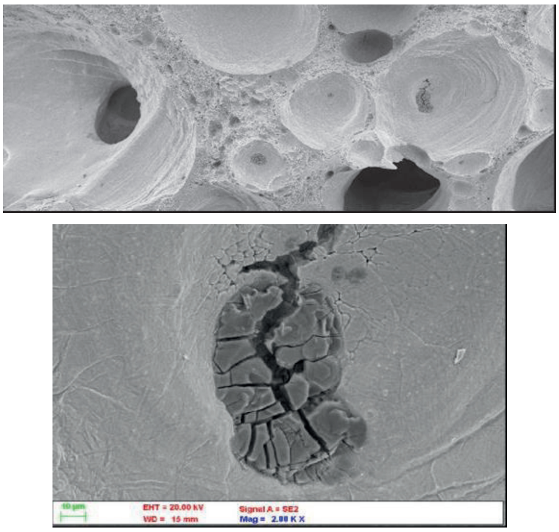

b)

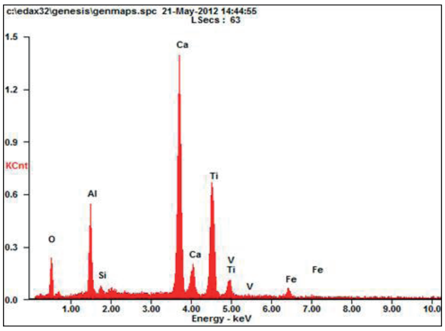

Fig. 15. Scanning electron micrograph SEM of clustered porosity on cross section of the bead-on-plate weld no. 16 (Table 2) (a) and EDS spectra of a pore bottom (b)

5. Conclusions

In contrast to the findings of other investigators, it was found that the dependence between the minimum heat input of laser welding, which is required for full penetration of the 5.0 mm plate of S700MC steel, is not a linear relationship, under the conditions of experiments such characteristic of the applied laser, and within the range of welding parameters. Results of the laser welding experiments clearly showed that the higher output power of the Disk laser beam the lower heat input required for full penetration of the steel plate.

Shape and depth/width ratio from 2 to 3 of all partially, and fully penetrated bead-on-plate welds, clearly show that the welds were produced at keyhole mode welding.

High susceptibility to form porosity during Disk laser welding of the S700MC steel was revealed. All of the partially penetrated bead-on-plate welds are characterized by "V" shape with intensive porosity in the region of weld root, but the porosity was found also in the upper part of FZ. Both a single pores, as well as clustered porosity were identified in the root region of weld metal. While the weld metal of fully penetrated bead-on-plate welds, shaped in "X" configuration, was almost free of porosity.

The tendency to form porosity in the weld metal during autogenous laser bead-on-plate welding is related not just to the speed of laser welding, but should be considered in relation to the heat input of laser welding. It was found that the lower heat input of laser welding the lower porosity of the weld metal. Therefore, in a case of welding at a given laser output power, the welding speed should be maximized to ensure a minimum heat input of welding.

Acknowledgment

The study was supported by the Innovation Center of NOT in Gliwice and Vlassenroot Polska, which is implementing the project POIG.01.04.00-24-052/13 (entitled "Technology of high productivity robotic welding in production of prototype device for underwater pipelines laying")

REFERENCES

[1] Rajashekhar S. Sharma, PalMolian, Weldability of advanced high strength steels using an Yb:YAG disk laser, Journal of Materials Processing Technology 211, 1888-1897 (2011).

[2] A. Grajcar, M. Różański, S. Stano, A. Kowalski, B. Grzegorczyk, Effect of Heat Input on Microstructure and Hardness Distribution of Laser Welded Si-Al TRIP-Type Steel, Adv. in Mat. Sci. and Eng. 2014 (2014).

[3] A. Lisiecki, Diode laser welding of high yield steel. Proceedings of SPIE, Laser Technology, Applications of Lasers 8703, 22 (2012).

[4] J. Górka, Analysis of simulated welding thermal cycles S700MC using a thermal imaging camera, Adv. Mat. Res. ISI Proceedings 837, 375-380 (2014).

[5] J. Górka, Influence of the maximum temperature of the thermal cycle on the properties and structure of the HAZ of steel S700MC, IOSR J. of Eng. 3(11), 22-28 (2013).

[6] M. Opiela, A. Grajcar, Hot deformation behavior and softening kinetics of Ti-V-B microalloyed steels, Arch. Civ. Mech. Eng. 12(3), 327-333 (2012).

[7] L.A. Dobrzański, A. Grajcar, W. Borek, Microstructure evolution of C-Mn-Si-Al-Nb high-manganese steel during the thermomechanical processing, Mat. Sci. Forum 638, 3224-3229 (2010).

[8] W. Sitek, J. Trzaska, L.A. Dobrzański, Modified Tartagli method for calculation of Jominy hardenability curve, Mat. Sci. Forum 575-578, 892-897 (2008).

[9] T. Węgrzyn, R. Wieszała, Main steel covered electrodes in terms of the Mount of oxygen in weld metal deposits (WMD), Metalurgija 51, 183-186 (2012).

[10] T. Węgrzyn, J. Piwnik, R. Wieszala, D. Hadryś, Control over the steel welding structure parameters by micro-jet cooling, Archives Of Metallurgy And Materials 57(3), 679-684 (2012).

[11] J. Slania, B. Slazak, M. Fidali, Application of fast fourier transform (FFT) in the analysis of a welding current instantaneous values waveforms during welding with a covered electrode, Arch. Metall. Mater. 59(2), 569-573 (2014).

[12] W. Sitek, A mathematical model of the hardness of high-speed steels, Transactions of Famena, 34 (3) 39-46 (2010).

[13] T. Węgrzyn, J. Mirosławski, A. Silva, D. Pinto, M. Miros, Oxide inclusions in steel welds of car body, Materials Science Forum 6, 585-591 (2010).

[14] T. Węgrzyn Mathematical Equations of the Influence of Molybdenum and Nitrogen in Welds. Conference of

International Society of Offshore and Polar Engineers ISOPE´2002, Kita Kyushu, Japan 2002, Copyright by International Society of Offshore and Polar Engineers, vol. IV, ISBN 1-880653-58-3, Cupertino – California – USA 2002.

[15] A. Kurc-Lisiecka, W. Ozgowicz, W. Ratuszek, J. Kowalska, Analysis of Deformation Texture in AISI 304 Steel Sheets, Sol. St. Phenomena 203-204, 105-110 (2013).

[16] K. Janerka, D. Bartocha, J. Szajnar, J. Jezierski, The carburizer influence on the crystallization process and the microstructure of synthetic cast iron, Arch. Metall. Mater. 55(3), 851-859 (2010).

[17] J. Kusiński, S. Kac, A. Kopia, A. Radziszewska, M. Rozmus-Górnikowska, B. Major, L. Major, J. Marczak, A.Lisiecki, Laser modification of the materials surface layer – a review paper. Bulletin of the Polish Academy of Sciences, Technical Sciences, 60(4), 711-728 (2012).

[18] K. Janerka, M. Pawlyta, J. Jezierski, J. Szajnar, D. Bartocha, Carburiser properties transfer into the structure of melted cast iron, J. Mat. Proc. Tech. 214(4), 2014 794-801.

[19] L.A. Dobrzański, M. Krupiński, K. Labisz, B. Krupińska, A. Grajcar: Phases and structure characteristics of the near eutectic Al-Si-Cu alloy using derivative thermo analysis, Materials Science Forum 638-642, 475-480 (2010).

[20] R. Burdzik, P. Folęga, B. Łazarz, Z. Stanik, J. Warczek, Analysis of the impact of surface layer parameters on wear intensity of frictional couples, Archives of Metallurgy and Materials **57** (4), 987-993 (2012).

[21] L. B l a c h a, Bleientfernung aus kupferlegierungen im prozess der vakuumraffination, Archives of Materials and Metallurgy 48 (1), 105-127 (2003).

[22] A. Fornalczyk, M. Saternus, Platinum recovery from used auto catalytic converters in electrorefining process. Metalurgija 52(2) 219-222 (2012).

[23] L. Blacha, R. Burdzik, A. Smalcerz, T. Matuła, Effects of pressure on the kinetics of manganese evaporation from the OT4 alloy, Archives Of Metallurgy And Materials **58** (1), 197-201 (2013).

[24] A. Kaźmierczak-Bałata, J. Bodzenta, D. Trefon-Radziejewska, Determination of thermal-diffusivity dependence on temperature of transparent samples by thermal wave method, International Journal of Thermophysics 31 (1), 180-186 (2010).

[25] J. Bodzenta, A. Kaźmierczak, T. Kruczek, Analysis of thermograms based on FFT algorithm, Journal de Physique IV 129, 201-206 (2005).

[26] A. Lisiecki: Welding of titanium alloy by Disk laser. Proceedings of SPIE, Laser Technology, Applications of Lasers, 87030 (2013).

[27] T. Węgrzyn The Classification of metal weld deposits in terms of the amount of nitrogen, Proceedings . Conference of International Society of Offshore and Polar Engineers ISOPE´2001, Stavanger, Norway 2001, International Society of Offshore and Polar Engineers, vol. IV, Cupertino – California, USA, 2001 282-285.

[28] T. Węgrzyn, J. Piwnik, R. Wieszała, D. Hadryś, Control over the steel welding structure parameters by micro-jet cooling, Archives of Metallurgy and Materials 57(1), 679-685 (2012).

[29] R. Burdzik, Ł. Konieczny, T. Figlus, Concept of on-board comfort vibration monitoring system for vehicles, J. Mikulski (Ed.): Activities of Transport Telematics, TST, CCIS 395, 418-425 (2013).

[30] R. Burdzik, Research on the influence of engine rotational speed to the vibration penetration into the driver via feet - multidimensional analysis, Journal of Vibroengineering 15(4), 2114-2123 (2013).

[31] Ł. Konieczny, R. Burdzik, B. Łazarz, Application of the vibration test in the evaluation of the technical condition of shock absorbers built into the vehicle, submitted to Journal of Vibroengineering 15(4), 2042-2048 (2013).

[32] R. Burdzik, Implementation of multidimensional identification of signal characteristics in the analysis of vibration properties of an automotive vehicle’s floor panel, Eksploatacja i Niezawodnosc – Maintenance and Reliability 16(3), 439-445 (2014).

[33] D. Janicki, Fiber laser welding of nickel based superalloy Rene 77, Proc. SPIE, Laser Technology 2012: Applications of Lasers, 2013, 8703, 87030Q, doi: 10.1117/12.2013428.

[34] D. Janicki, Fiber laser welding of nickel based superalloy Inconel 625, Proc. SPIE, Laser Technology 2012: Applications of Lasers, 2013, 8703, 87030R, doi: 10.1117/12.2013430.

[35] L.A. Dobrzański, M. Bonek, M. Piec, E. Jonda, Diode laser modification of surface gradient layer properties of a hot-work tool steel, Mat. Sci. Forum (532-533) 657-660 (2006).

[36] M. Musztyfaga, L.A. Dobrzański, S. Rusz, M. Staszuk, Application examples for the different measurement modes of electrical properties of the solar cells, Arch. Metall. Mater. 59(1), 247-252 (2014).

[37] R. Burdzik, Ł. Konieczny, Z. Stanik, P. Folega, A. Smalcerz, A. Lisiecki, Analysis of impact of chosen parameters on the wear of camshaft, Arch. Metall. Mater. 59(3), 961-967 (2014).

[38] M. Urzynicok, K. Kwiecinski, J. Slania, Analysis of problems occured during welding of new genreation bainitic steel 7CrMoVTiB10-10 (T24), Arch. Metall. Mater. 58(3), 691-696 (2013).

[39] A. Klimpel, A. Lisiecki, A. Szymanski, A.P. Hoult, Numerical and experimental determination of weld pool shape during high-power diode laser welding, Proc. of SPIE Vol. 5229, Laser Technology VII: Applications of Lasers, 6 Oct. 2003, pp. 247-250, doi:10.1117/12.520726.

[40] J.T. Norris, C.V. Robino, D.A. Hirschfeld, M.J. Perricone, Effects of Laser Parameters on Porosity Formation: Investigating Millimeter Scale Continuous Wave Nd:YAG Laser Welds, Welding Journal 90, 198-203 (2011).

[41] M.J. Torkamany, J. Sabbaghzadeh, M.J. Hamedi, Effect of laser welding mode on the microstructure and mechanical performance of dissimilar laser spot welds between low carbon and austenitic stainless steels, Materials and Design 34, 666-672 (2012).

[42] J. Słania, Influence of phase transformations in the temperature ranges of 1250-1000ºC and 650-350ºC on the ferrite content in austenitic welds made with T 23 12 LRM3 tubular electrode. Archives of Metallurgy and Materials **50**(3), 757-767(2005).

Received: 10 January 2015.